THE JOURNAL OF BIOLOGICAL CHEMISTRY VOL. 282, NO. 47, pp. 34229–34234, November 23, 2007

MCM Forked Substrate Specificity Involves Dynamic Interaction with the 5′-Tail*[S]

Received for publication, July 31, 2007, and in revised form, September 10, 2007 Published, JBC Papers in Press, September 20, 2007, DOI 10.1074/jbc.M706300200

Eli Rothenberg[‡1], **Michael A. Trakselis**[§2], **Stephen D. Bell**[§], **and Taekjip Ha**[‡¶3]

From the [‡]*Department of Physics and the* [¶]*Howard Hughes Medical Institute, University of Illinois at Urbana-Champaign, Urbana, Illinois 61801 and the* [§]*Medical Research Council Cancer Cell Unit, Hutchison Medical Research Council Research Center, Hills Road, Cambridge CB2 2XZ, United Kingdom*

The archaeal minichromosome maintenance protein MCM forms a homohexameric complex that functions as the DNA replicative helicase and serves as a model system for its eukaryotic counterpart. Here, we applied single molecule fluorescence resonance energy transfer methods to probe the substrate specificity and binding mechanism of MCM from the hyperthermophilic Archaea *Sulfolobus solfataricus* on various DNA substrates. *S. solfataricus* MCM displays a binding preference for forked substrates relative to partial or full duplex substrates. Moreover, the nature of MCM binding to Y-shaped substrates is distinct in that MCM loads on the 3′-tail while interacting with the 5′-tail likely via the MCM surface. These results provide the first elucidation of a dynamic nature of interaction between a ring-shaped helicase interacting with an opposing single-stranded DNA tail. This interaction contributes to substrate selectivity and increases the stability of the forked DNA-MCM complex, with possible implications for the MCM unwinding mechanism.

The eukaryotic minichromosome maintenance MCM2–7 complex plays a vital role in replication and is thought to be the replicative helicase (1, 2). MCM2–7 is involved in various stages of the replication process, from licensing through initiation, replication, and termination (3, 4). The MCM2–7 complex forms a heterohexamer, with a subcomplex (MCM4-6-7) functioning as a 3′–5′-helicase. The six subunits possess sequence similarity, suggesting a common evolutionary origin (1, 5). The archaeal replication process represents a simpler form of that found in the Eukarya (6) and provides an excellent model system for studying replication (7, 8). Most archaeal species encode a single MCM that is homologous to its eukaryotic counterparts (9) and that forms a homohexamer (10, 11) or a double homohexamer (12).

The binding, translocation, and unwinding mechanisms of archaeal and eukaryotic MCM protein, and other replicative helicases have been the focus of many research efforts (13–15). MCM4-6-7 DNA unwinding shows a requirement for Y-shaped DNA substrate (16) or a 3′-tailed DNA with a 5′-bulky attachment (17), leading to the double hexamer model and steric exclusion model, respectively. Archaeal MCM proteins also display enhanced unwinding of a forked DNA substrate (18–20). The importance of the opposing strand in efficient DNA unwinding is also evident in 5′–3′-replicative helicases such as *Escherichia coli* DnaB helicase (21) and bacteriophage T7 helicase (22). Although it is clear that a forked DNA is the unwinding substrate preferred by replicative helicases, debate exists over the nature and functional role of interactions between the enzyme and the single-stranded (ssDNA)[4] and double-stranded DNA components of the substrate, and many of the subtleties regarding replicative helicase binding, unwinding, and translocation remain elusive (13, 14, 23).

Single molecule techniques can reveal inner details of biochemical reactions and have been used to study mechanisms of various helicases (24–30). Herein, we report on the mechanism of DNA binding and substrate selectivity of *Sulfolobus solfataricus* MCM (*Sso*MCM) obtained through single molecule fluorescence resonance energy transfer (smFRET) studies. smFRET (31, 32) is a powerful method able to unravel biological events, including helicase activities, without ensemble averaging. smFRET was applied to probe the binding and orientation of MCM on DNA as well as the conformational changes induced in DNA upon MCM loading. MCM demonstrates a specificity of binding to forked DNA over single-tailed and duplex substrates. This results from a highly dynamic interaction between the 5′-tail and MCM, with a mechanistic implication on replicative helicases.

EXPERIMENTAL PROCEDURES

DNA Substrates and Annealing—Oligonucleotide substrates were purchased from Integrated DNA Technologies (Coralville, IA). Forked, partial, and duplex substrates were prepared by mixing the biotinylated and non-biotinylated strands

* This work was supported in part by National Institutes of Health Grant GM065367 (to T. H.) and by the Medical Research Council (to S. D. B.). The costs of publication of this article were defrayed in part by the payment of page charges. This article must therefore be hereby marked "*advertisement*" in accordance with 18 U.S.C. Section 1734 solely to indicate this fact.

[S] The on-line version of this article (available at http://www.jbc.org) contains supplemental "Experimental Procedures," Equations 1–4, Figs. 1 and 2, and a table.

[1] Supported by a European Molecular Biology Organization long-term fellowship.

[2] Present address: Dept. of Chemistry, University of Pittsburgh, Pittsburgh, PA 15260.

[3] Investigator with the Howard Hughes Medical Institute. To whom correspondence should be addressed: Dept. of Physics, Howard Hughes Medical Inst., University of Illinois at Urbana-Champaign, 1110 West Green St., Urbana, IL 61801. Tel.: 217-265-0717; Fax: 217-244-7187; E-mail: tjha@uiuc.edu.

[4] The abbreviations used are: ssDNA, single-stranded DNA; *Sso*MCM, *S. solfataricus* MCM; smFRET, single molecule fluorescence resonance energy transfer.

in a 1:1.5 ratio at 1 μM in buffer containing 10 mM Tris (pH 8) and 200 mM NaCl. The non-biotinylated strand was added in excess to minimize the chance of having residual biotinylated strand in the measurement. The annealing mixture was heated at 95 °C for 2 min and allowed to cool slowly for 2 h in the heating block. (For substrates and sequences, see supplemental "Experimental Procedures.")

Protein Purification and Protein Labeling—Wild-type *Sso*MCM and its C642A mutant were purified as described previously (10). Cy3 and Cy5 *N*-hydroxysuccinimide esters and maleimides were purchased from GE Healthcare. Fluorescence labeling of *Sso*MCM was also performed as described previously (10). Briefly, wild-type *Sso*MCM was incubated with the *N*-hydroxysuccinimide ester in 25 mM HEPES, 150 mM NaCl, and 10 mM $MgCl_2$ at pH 6.8 and then quenched with 10 mM Tris after 1 h (referred to as N-MCM). C642A mutant *Sso*MCM was incubated with the maleimide in the same buffer at pH 7.5 and then quenched with 10 mM β-mercaptoethanol after 4 h (referred to as C-MCM). Labeled MCM proteins were spun through a spin column and dialyzed extensively to remove any remaining free label. The degree of labeling was determined by UV spectrometry using the appropriate extinction coefficients and found to be essentially 1 for all cases.

Single Molecule Spectroscopy—smFRET measurements were performed using a wide-field total internal reflection fluorescence microscope (33, 34). Total internal reflection excitation was done either using a prism or through an objective (Olympus UPlanSApo ×100 numerical aperture 1.4 oil). Images were acquired with a 30-ms time resolution using an electron-multiplying charge-coupled device camera (iXon DV887-BI, Andor Technology) and a homemade C++ program. FRET values were calculated as the ratio between the acceptor intensity and the sum of the intensities of the donor and acceptor, after correcting for cross-talk between the two detection channels and subtracting the background (32, 35).

A quartz slide was coated with polyethylene glycol, with 1–2% (w/w) biotin-polyethylene glycol (34, 35). Surface integrity and nonspecific binding were tested by separately adding Cy3-labeled protein (4 μM) and DNA (1 nM). Once surface integrity was verified, NeutrAvidin was added as described (32, 35), followed by immobilizing biotinylated DNA (150 pM). All measurements were performed at room temperature with buffer 4 from New England Biolabs (Ipswich, MA), which contains 50 mM potassium acetate, 20 mM Tris acetate, 10 mM magnesium acetate, and 1 mM dithiothreitol (pH 7.9). The buffer also contained 0.8% glucose with an oxygen scavenger system (0.1 mg/ml glucose oxidase, 0.02 mg/ml catalase, 1% β-mercaptoethanol, and 0.4% (w/w) β-D-glucose) (32, 35).

Single Molecule Measurements of Labeled MCM Complex—To reduce the possibility of FRET between one-donor DNA and an MCM hexamer labeled with multiple acceptors, wild-type MCM was mixed with labeled MCM to yield a final labeled/unlabeled monomer ratio of 1:8. Labeled and unlabeled MCM proteins were incubated in the dark for at least 1 h at room temperature.

Surface-attached DNA molecules were incubated with the reported concentrations of MCM (all given in *monomer* concentration) for 5 min, ensuring sufficient time for binding. Excess and unbound MCM was removed by a wash with buffer 4, followed by a wash with imaging buffer.

RESULTS

smFRET Analysis of SsoMCM Fork Binding Orientation—*Sso*MCM contains several functional domains with separable domain-dependent activities. The C-terminal half contains the AAA^+ (ATPases associated with a variety of cellular activities) domain and a helix-turn-helix motif, and the N terminus includes the Walker A and B motifs (10). Recent studies of truncated *Sso*MCM complexes assigned the helicase activity to the C-terminal half and showed that the N-terminal half governs substrate selectivity and enzyme processivity (36).

For smFRET measurements, Cy3 was used as the donor and Cy5 as the acceptor. For DNA-to-MCM FRET analysis, MCM was labeled with Cy5 at the N terminus (N-MCM) or C terminus (C-MCM), and the various DNA substrates were labeled with Cy3. The activity of purified and labeled MCM was verified prior to measurements as described (10). The DNA molecules were attached to the surface of a flow chamber and incubated with MCM at a specified *monomer* concentration, followed by an extensive wash to remove unbound MCM (see "Experimental procedures"). The orientation of MCM was measured via the binding of acceptor-labeled C-MCM or N-MCM (8 μM prewash *monomer* concentration) to forked DNA substrates that were donor-labeled at either the 3′-end or the junction. The normalized relative distance distributions, extracted from smFRET efficiency histograms, are shown for four different combinations: N terminus to 3′-end, C terminus to 3′-end, C terminus to junction, and N terminus to junction (Fig. 1, *A–D*, respectively). The data indicate that the N terminus is closer to the 3′-end (~5.4 nm) than to the junction (>8.2 nm). The distances were calculated using the previously determined value of ~6.3 nm for the Cy3–Cy5 pair (35) and should be considered only as an approximation because of the relatively large fluorescence anisotropy of the protein- and DNA-conjugated fluorophores. Additionally, the C terminus is closer to the junction (~7.0 nm) than to the N terminus (>8.2 nm). In combination, our data indicate the MCM orientation illustrated in Fig. 1; MCM binds to the 3′-tail with the C-terminal AAA^+ helicase domain facing the junction and the N-terminal domain, which includes the substrate selectivity domain, closer to the 3′-end. These findings are in agreement with the previously reported organization of MCM on DNA (10) as measured in ensemble experiments, validating our smFRET assays.

SsoMCM Substrate Binding Specificity—We next aimed to probe the substrate binding preference of MCM. The fluorescence of surface-tethered donor-labeled DNA, either forked or with a 3′-tail (Fig. 2*B*), was measured after incubation with 3 μM acceptor-labeled C-MCM. Fig. 2*A* shows donor (*panel I*) and acceptor (*panel II*) single molecule fluorescence images of MCM bound to forked DNA (*panel I*) and the single 3′-tailed partial duplex (*panel II*). The fraction of DNA bound by MCM was determined from the resulting smFRET histograms (see supplemental "Experimental Procedures"). MCM displayed a nearly 2-fold enhanced binding to forked DNA substrate over the 3′-tailed partial duplex substrates (Fig. 2*B*). We considered the following three explanations at to why MCM prefers a

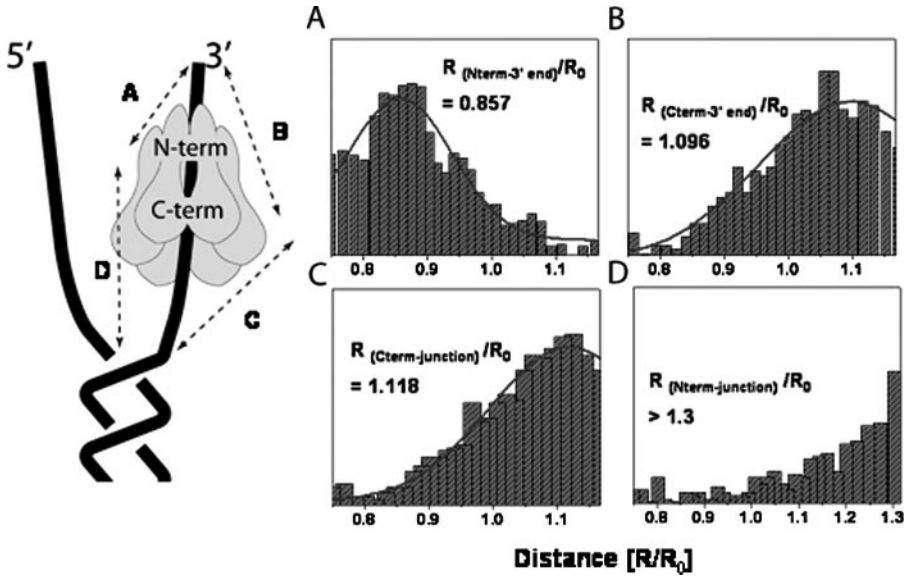

FIGURE 1. **Orientation of MCM bound on forked DNA.** The average relative distance (R/R_0) was calculated from smFRET efficiency histograms (see supplemental "Experimental Procedures") obtained following the incubation of 8 μM MCM and extensive washing. FRET was measured between the following pairs: 3′-end and N terminus (*N-term*) (*A*), 3′-end and C terminus (*C-term*) (*B*), junction and C terminus (*C*), and junction and N terminus (*D*). The organization of MCM on the fork is illustrated on the left.

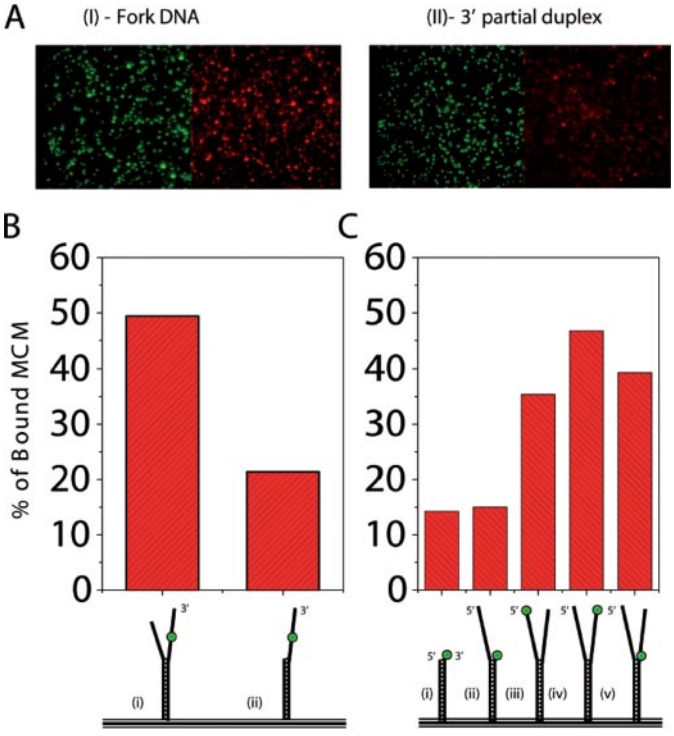

FIGURE 2. **MCM showing preferences for forked substrates.** *A*, representative single molecule acceptor-donor fluorescence images of the binding of acceptor-labeled MCM to the donor-labeled forked (*panel I*) and single 3′-tailed (*panel II*) DNAs. The *green spots* in each image correspond to donor molecule fluorescence (Cy3-DNA 3′-tail), and the *red spots* correspond to acceptor (Cy5-MCM). *B*, binding efficiency of the forked and single 3′-tailed substrates calculated from smFRET efficiency histograms. *C*, binding efficiency for the five other substrates, as shown below, calculated from smFRET efficiency histograms.

forked DNA: 1) MCM loads on the free 3′-tail while externally grabbing the 5′-tail, possibly through surface binding modes; 2) MCM preferentially encircles both the 3′- and 5′-tails in its central channel; and 3) as proposed previously for MCM (37), two hexamers are arranged in an eccentrically stacked double hexamer and bind separately to the 3′- and 5′-tails, each with its own polarity such that binding is improved when both tails are present.

To distinguish among these binding modes, we determined the efficiency of binding of MCM to other substrates. Five different donor-labeled substrates were measured: an 18-bp full duplex, a 5′-tailed partial duplex, and three forked substrates labeled in different locations (Fig. 2*C*). Binding efficiency was low for the full duplex and 5′-tailed duplex substrates and was significantly higher for the forked substrates (Fig. 2*C*). The low binding of MCM to duplex substrates disfavors the second loading mechanism. Hence, the observed MCM preferred loading on forked substrates may be either due to external binding of the 5′-tail or through a double hexamer binding both strands.

To further probe the loading mechanism, we designed three forked substrates labeled with a donor and an acceptor on opposing tails (Fig. 3), enabling us to investigate the behavior of the forked tails upon MCM loading. The DNA substrates were tethered to the surface, and unlabeled MCM at the indicated concentration was added (see "Experimental Procedures"). Fig. 3*A* shows the smFRET efficiency histograms of a forked DNA substrate with a donor at the 3′-tail end and an acceptor at the 5′-tail end as a function of MCM concentration. DNA showed only low FRET efficiency values (Fig. 3*A*, *upper panel*) because of a large separation of flexible ssDNA. With increasing MCM concentrations, higher FRET efficiency populations emerged, indicating that the 3′- and 5′-tails are being brought closer together. This effect was also observed with two other forked substrates with similarly labeled 5′-tails, but with longer and internally labeled 3′-tails (Fig. 3, *B* and *C*). The existence of a high FRET efficiency population even at an MCM concentration as low as 150 nM is indicative of a single MCM hexamer bound on the forked substrates, not double hexamers, because previous stoichiometric analyses showed that *Sso*MCM assembles on a forked DNA only as a hexamer at concentrations up to 5 μM (10, 18). In addition, double hexamer loading would yield low FRET because the DNA tails would be spatially separated by the proteins. These results led us to propose that the 3′-tail of the forked DNA substrate is accommodated in the central channel of the MCM hexamer, whereas the DNA 5′-tail binds externally (Fig. 3*D*).

MCM Fork Binding and Interactions with the Opposite Strand—We next examined the dynamic nature of MCM binding to the forked DNA. To test the stability of the DNA-MCM complex, forked DNA (Fig. 3, *substrate 1*) was incubated with 4 μM MCM, washed, and monitored for >1 h (supplemental Fig.

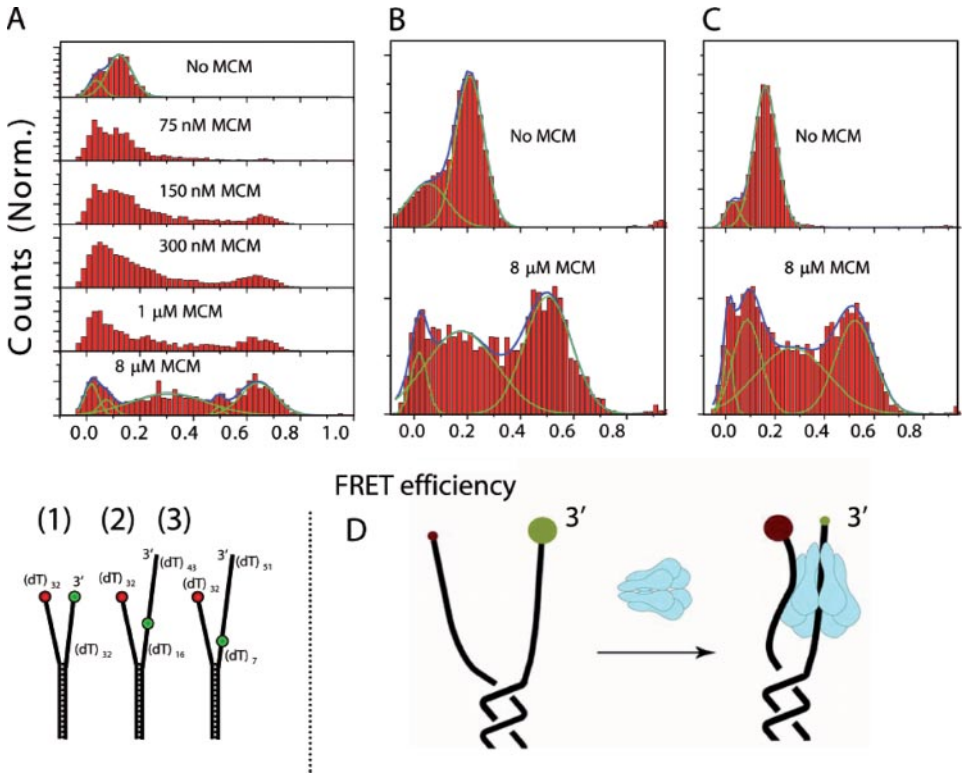

FIGURE 3. **Binding of MCM on forked substrates and interaction with the 5′-tail.** The three forked *substrates 1–3* are shown. *A*, smFRET efficiency histograms of *substrate 1* as a function of MCM concentration. Peaks at FRET = 0 are due to inactive or missing acceptor molecules. *B*, same as *A* but for *substrate 2*. *C*, same as *A* but for *substrate 3*. *D*, illustration of MCM loading on fork DNA. In the absence of MCM, the donor and acceptor are far apart, whereas upon MCM loading, the tails are brought closer together, resulting in FRET increase. *Norm.*, normalized.

1). No significant dissociation of MCM from the DNA was observed, ensuring that our measurements were not influenced by protein dissociation.

Individual DNA molecules bound by MCM displayed temporal fluctuations in FRET efficiency in the absence of free MCM in solution (Fig. 4*A*, *panel I*), likely representing distance changes between the two ends of the forked substrate. Such continual fluctuation in distance with no apparent regularity was observed for the majority of molecules with all three forked substrates (81, 82, and 74% for *substrates 1–3*, respectively, in Fig. 3) and was still detected after ATP was added (supplemental Fig. 2). Similar behavior was observed for FRET efficiency between the donor at the 5′-tail and the acceptor at the N terminus of MCM (Fig. 4*A*, *panel II*), indicating a dynamic interaction of the 5′-tail with MCM. Furthermore, such complex interaction with MCM is unique to the 5′-tail, as we did not observe similar fluctuations in FRET between a donor at the 3′-tail and an acceptor on MCM.

To further analyze this phenomenon, having no apparent regular fluctuation period or amplitude, we applied an autocorrelation analysis, in which, by self-correlating the values of a FRET efficiency time trace at different time periods, the characteristic relaxation times and behaviors can be extracted (see supplemental "Experimental Procedures"). The autocorrelation functions of individual smFRET traces were calculated and averaged over many molecules, ranging from 20 to 100 molecules for each experiment, to extract the characteristic time scales (Fig. 4*B*). Both the MCM-induced tail/tail interactions (Fig. 4*B*, *panels I–III*) and the 5′-tail/MCM interaction (*panel IV*) yielded average autocorrelation functions of similar shapes and times scales. The autocorrelation fitted poorly with an exponential decay function (Fig. 4*B*, *panel I*, *blue curve*), whereas a stretched exponential type function (Fig. 4*B*, *red curves*), modeled previously for subdiffusion phenomena (38–40), provided a good fit. The relaxation time was in the second range but with stretch coefficients of ~0.5, indicating a wide range of time scales for the dynamics, ranging from 60 ms to 5 s (Fig. 4*B* and supplemental "Experimental Procedures"). Subdiffusion is an anomalous diffusion phenomenon in which the mean square displacement has sublinear dependence on time, in contrast to regular diffusion with linear dependence on time (38, 40, 41). Our analysis therefore indicates that the interaction between the 5′-tail and MCM surface can occur in many conformational states, each with a unique trapping and relaxation time, resulting in an interaction governed by subdiffusion kinetics.

DISCUSSION

Using smFRET, we found that MCM possesses specificity for forked DNA substrates over single-tailed and duplex substrates. Furthermore, MCM loads on the forked DNA 3′-tail, with its C terminus facing the junction and N terminus toward the 3′-end, and externally binds to the 5′-tail. Previous ensemble FRET analysis of *Sso*MCM deduced the same binding orientation; however, a recent crystal structure of another hexameric AAA^+ helicase, papillomavirus E1, shows binding to an ssDNA with opposite polarity (42). Our smFRET result further supports the apparent difference in DNA binding polarity between *Sso*MCM and papillomavirus E1.

The interaction between the 3′-tail-bound MCM complex and the 5′-tail was found to be dynamic, with fluctuations occurring on wide distance and time scales. This suggests that the 5′-tail does not simply bind the MCM surface and fall off, but instead experiences an intricate interaction landscape. Assuming there exists at least one external binding site in each monomer, the MCM hexamer would involve at least six such binding sites, with many possible conformations of the 5′-tail onto these sites. We propose that the external 5′-tail/MCM interaction is weak per binding site, enabling the 5′-tail to break off and diffuse between different sites. The diffusion steps between the different binding sites will therefore depend on the 5′-tail conformation and its arrangement on the various sites,

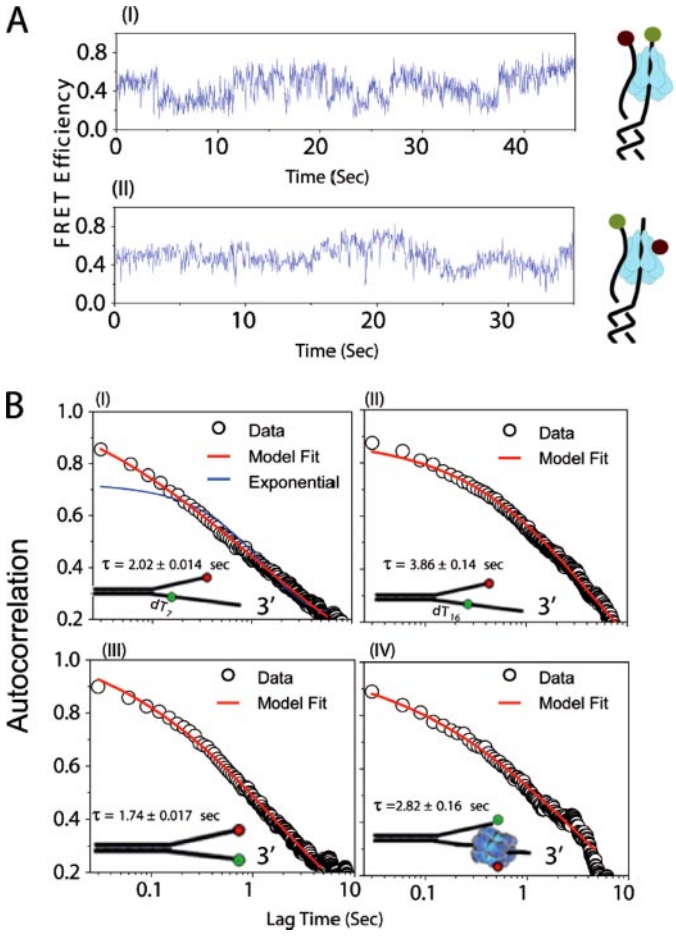

FIGURE 4. **Dynamics of the MCM-bound forked substrate.** *A*, representative smFRET efficiency time traces between the labeled 5′-tail (acceptor) and the 3′-tail (donor) with bound MCM (*panel I*) and between the labeled 5′-tail (donor) and N-terminally labeled MCM (acceptor) bound on the 3′-tail (*panel II*). *B*, averaged autocorrelation functions calculated for the three forked substrate FRET pairs and the MCM 5′-tail FRET pair obtained from 104 (*panel I*), 63 (*panel II*), 40 (*panel III*), and 21 (*panel IV*) molecules.

with additional contributing factors such as ssDNA strain and the location of MCM on the 3′-tail. The net result would be a shallow but rugged energy landscape with many possible local minima, which would increase the stability of MCM on the replication fork and determine the distinctive selectivity of MCM for forked substrates.

The architecture of replicative helicases at the replication fork during DNA unwinding has been the subject of much debate. Some of the various suggested models are passive unwinding, in which the helicase translocates on one ssDNA and awaits the opening of the junction to translocate forward; and several dynamic models, in which the helicase directly destabilizes the junction (3, 13, 14, 26, 43). For MCM, diverse models have been proposed, including steric exclusion, rotary pump, T-antigen, and Ploughshare (23, 37, 44), suggesting an interaction with either single- or double-stranded DNA. In the steric exclusion model, the opposing strand (5′-tail) prevents the helicase from encircling and translocating along the duplex DNA and does not play an additional role once the helicase starts unwinding the DNA. In contrast, our data show that *Sso*MCM dynamically interacts with the 5′-end, which should also be the case during duplex unwinding. Such dynamic interaction between a ring-shaped helicase and an opposing ssDNA tail has not been elucidated previously.

In light of our findings, we propose the following "opposite strand interaction" model for MCM/replication fork association. MCM loads with the 3′-tail accommodated in its central channel, and the 5′-tail binds and diffuses on its surface. This interaction would regulate the binding specificity for forked substrates and aid in the long-term stability of the MCM-replication fork complex and replication fidelity. It should be noted that the weak interaction of MCM with the opposite strand may be beneficial in preventing tangling of ssDNA or stalled replication by ensuring that the interaction is local, whereas it is possible that a single strand binding protein (single-stranded DNA-binding protein or replication protein A) also aids in preventing the MCM surface from binding to ssDNA at a distance. Additionally, as a 3′–5′-helicase MCM will translocate along the leading strand template (3′-tail), its dynamic interaction with the unwound lagging strand template (5′-tail) may facilitate coordination of leading and lagging strand synthesis events. In this regard, it may be relevant that the DNA primase-binding archaeal GINS complex interacts with the trailing N-terminal domains of *Sso*MCM (45). Additionally, this type of interaction may be incorporated into the unwinding mechanism of MCM, in which upon ATP hydrolysis, MCM will translocate forward on the ssDNA while drawing the 5′-tail. This combined forward translocation and opposite strand binding may result in sufficient destabilization of the junction, facilitating double-stranded DNA unwinding. Finally, we should also consider the possibility that the observed interaction may have inhibitory effects on the helicase activity (46), which may be lifted if another protein such as the DNA polymerase occupies the opposing strand (47, 48).

Our smFRET study has revealed unique information about dynamic interaction between MCM and the opposite strand in the context of replication fork association with MCM. These findings likely bear relevance to the mechanism of replication fork binding and unwinding by MCM and other replicative helicases.

REFERENCES

1. Forsburg, S. L. (2004) *Microbiol. Mol. Biol. Rev.* **68,** 109–131
2. Bell, S. P., and Dutta, A. (2002) *Annu. Rev. Biochem.* **71,** 333–374
3. Maiorano, D., Lutzmann, M., and Mechali, M. (2006) *Curr. Opin. Cell Biol.* **18,** 130–136
4. Lindner, K., Gregan, J., Montgomery, S., and Kearsey, S. E. (2002) *Mol. Biol. Cell* **13,** 435–444
5. Johnson, A., and O'Donnell, M. (2005) *Annu. Rev. Biochem.* **74,** 283–315
6. Barry, E. R., and Bell, S. D. (2006) *Microbiol. Mol. Biol. Rev.* **70,** 876–887
7. Duggin, I. G., and Bell, S. D. (2006) *J. Biol. Chem.* **281,** 15029–15032
8. Kelman, Z., and White, M. F. (2005) *Curr. Opin. Microbiol.* **8,** 669–676
9. Kelman, L. M., and Kelman, Z. (2003) *Mol. Microbiol.* **48,** 605–615
10. McGeoch, A. T., Trakselis, M. A., Laskey, R. A., and Bell, S. D. (2005) *Nat. Struct. Mol. Biol.* **12,** 756–762
11. Chen, Y. J., Yu, X. O., Kasiviswanathan, R., Shin, J. H., Kelman, Z., and Egelman, E. H. (2005) *J. Mol. Biol.* **346,** 389–394
12. Fletcher, R. J., Bishop, B. E., Leon, R. P., Sclafani, R. A., Ogata, C. M., and Chen, X. J. S. (2003) *Nat. Struct. Biol.* **10,** 160–167
13. Patel, S. S., and Donmez, I. (2006) *J. Biol. Chem.* **281,** 18265–18268
14. Donmez, I., and Patel, S. S. (2006) *Nucleic Acids Res.* **34,** 4216–4224
15. Yu, Z. L., Feng, D. R., and Liang, C. (2004) *J. Mol. Biol.* **340,** 1197–1206
16. Lee, J. K., and Hurwitz, J. (2001) *Proc. Natl. Acad. Sci. U. S. A.* **98,** 54–59

17. Kaplan, D. L., Davey, M. J., and O'Donnell, M. (2003) *J. Biol. Chem.* **278,** 49171–49182
18. Carpentieri, F., De Felice, M., De Falco, M., Rossi, M., and Pisani, F. M. (2002) *J. Biol. Chem.* **277,** 12118–12127
19. Haugland, G. T., Shin, J. H., Birkeland, N. K., and Kelman, Z. (2006) *Nucleic Acids Res.* **34,** 6337–6344
20. Shin, J. H., Jiang, Y., Grabowski, B., Hurwitz, J., and Kelman, Z. (2003) *J. Biol. Chem.* **278,** 49053–49062
21. Galletto, R., Jezewska, M. J., and Bujalowski, W. (2004) *J. Mol. Biol.* **343,** 101–114
22. Jeong, Y. J., Levin, M. K., and Patel, S. S. (2004) *Proc. Natl. Acad. Sci. U. S. A.* **101,** 7264–7269
23. Delagoutte, E., and von Hippel, P. H. (2002) *Q. Rev. Biophys.* **35,** 431–478
24. Myong, S., Rasnik, I., Joo, C., Lohman, T. M., and Ha, T. (2005) *Nature* **437,** 1321–1325
25. Myong, S., Bruno, M. M., Pyle, A. M., and Ha, T. (2007) *Science* **317,** 513–516
26. Johnson, D. S., Bai, L., Smith, B. Y., Patel, S. S., and Wang, M. D. (2007) *Cell* **129,** 1299–1309
27. Dohoney, K. M., and Gelles, J. (2001) *Nature* **409,** 370–374
28. Dumont, S., Cheng, W., Serebrov, V., Beran, R. K., Tinoco, I., Pyle, A. M., and Bustamante, C. (2006) *Nature* **439,** 105–108
29. Spies, M., Bianco, P. R., Dillingham, M. S., Handa, N., Baskin, R. J., and Kowalczykowski, S. C. (2003) *Cell* **114,** 647–654
30. Dessinges, M. N., Lionnet, T., Xi, X. G., Bensimon, D., and Croquette, V. (2004) *Proc. Natl. Acad. Sci. U. S. A.* **101,** 6439–6444
31. Ha, T., Enderle, T., Ogletree, D. F., Chemla, D. S., Selvin, P. R., and Weiss, S. (1996) *Proc. Natl. Acad. Sci. U. S. A.* **93,** 6264–6268
32. Ha, T. (2001) *Methods* (*San Diego*) **25,** 78–86
33. Zhuang, X. W., Bartley, L. E., Babcock, H. P., Russell, R., Ha, T. J., Herschlag, D., and Chu, S. (2000) *Science* **288,** 2048–2051
34. Ha, T., Rasnik, I., Cheng, W., Babcock, H. P., Gauss, G. H., Lohman, T. M., and Chu, S. (2002) *Nature* **419,** 638–641
35. Rasnik, I., Myong, S., Cheng, W., Lohman, T. M., and Ha, T. (2004) *J. Mol. Biol.* **336,** 395–408
36. Barry, E. R., McGeoch, A. T., Kelman, Z., and Bell, S. D. (2007) *Nucleic Acids Res.* **35,** 988–998
37. Takahashi, T. S., Wigley, D. B., and Walter, J. C. (2005) *Trends Biochem. Sci.* **30,** 437–444
38. Yang, H., and Xie, X. S. (2002) *J. Chem. Phys.* **117,** 10965–10979
39. Metzler, R., Barkai, E., and Klafter, J. (1999) *Phys. Rev. Lett.* **82,** 3563–3567
40. Metzler, R., and Klafter, J. (2000) *Phys. Rep. Rev. Sec. Phys. Lett.* **339,** 1–77
41. Yang, H., Luo, G. B., Karnchanaphanurach, P., Louie, T. M., Rech, I., Cova, S., Xun, L. Y., and Xie, X. S. (2003) *Science* **302,** 262–266
42. Enemark, E. J., and Joshua-Tor, L. (2006) *Nature* **442,** 270–275
43. Donmez, I., Rajagopal, V., Jeong, Y. J., and Patel, S. S. (2007) *J. Biol. Chem.* **282,** 21116–21123
44. von Hippel, P. H., and Delagoutte, E. (2003) *BioEssays* **25,** 1168–1177
45. Marinsek, N., Barry, E. R., Makarova, K. S., Dionne, I., Koonin, E. V., and Bell, S. D. (2006) *EMBO Rep.* **7,** 539–545
46. Ha, T. (2007) *Cell* **129,** 1249–1250
47. Stano, N. M., Jeong, Y. J., Donmez, I., Tummalapalli, P., Levin, M. K., and Patel, S. S. (2005) *Nature* **435,** 370–373
48. Lee, J. B., Hite, R. K., Hamdan, S. M., Xie, X. S., Richardson, C. C., and van Oijen, A. M. (2006) *Nature* **439,** 621–624